On critical dependence of atmospheric circulation response to regional SST biases on background SST

Yuan-Bing Zhao[1], Nedjeljka Žagar[1], and Frank Lunkeit[1]

[1]Meteorologisches Institut, Universität Hamburg, Hamburg, Germany

Key Points:

- The global atmospheric response to regional SST biases varies significantly across regions.
- The response is defined by the critical threshold of the background SST for intense convection.
- Results highlight the importance of regions with background $SST > 26°C$ in climate models.

Corresponding author: Yuan-Bing Zhao, yuan-bing.zhao@uni-hamburg.de

Abstract

This study examines how the geographic location of sea surface temperature (SST) biases influences global atmospheric responses. Utilizing an intermediate-complexity atmospheric model, 106 century-long simulations with idealized SST perturbations—emulating biases in coupled climate models—were performed. The intensity of the global atmospheric response to SST biases is evaluated by quantifying changes in global wave energy and interannual variance. The findings underscore the response's dependency on local background SST. Notably, with an imposed SST bias of +1.5 K, a significant global response is triggered once background SST surpasses approximately 25°C. This geographic dependency is related to the critical SST threshold for intense convection. Consequently, these results highlight the need for heightened focus on tropical oceans, especially the Indo-West Pacific, where SST biases can significantly impact the accuracy of global climate simulations.

Plain Language Summary

Understanding the impact of sea surface temperature (SST) biases on simulated atmospheric circulation is crucial for uncertainty quantification in climate projection. Here, we investigate the impact of regional SST biases on the model atmosphere and how this impact varies with the geographic location of the SST bias. We performed 106 idealized century-long sensitivity simulations with an intermediate complex atmospheric model. Based on these simulations, we assessed the effect of regional SST biases on the global atmospheric circulation using a novel dynamical approach, which enables us to quantify the changes in global spatio-temporal variability. The amplitude of the global atmospheric response to regional SST biases is found to depend strongly on the local background SST. SST biases in warmer tropical oceans have much stronger impacts than those in cooler extratropical oceans. In particular, given an SST bias of +1.5 K, there is a substantial response when the local background SST exceeds approximately 25°C.

1 Introduction

State-of-the-art coupled climate models often have difficulty accurately representing sea surface temperature (SST) in their historical simulations, leading to pronounced SST biases (e.g., Wang et al., 2014; Burls et al., 2017; Zhu et al., 2020; Wills et al., 2022; Q. Zhang et al., 2023). Understanding how these SST biases affect the simulated atmospheric variability is a key element of uncertainty quantification of climate prediction.

SST biases can influence regional atmospheric circulation in various ways. For instance, SST biases in the tropical Indian Ocean alter the meridional SST gradient, subsequently impacting the Indian Summer Monsoon (e.g., Joseph et al., 2012; Prodhomme et al., 2014). Excessively warm SSTs in the tropical Southeast Pacific and Atlantic are responsible for a spurious double intertropical convergence zone (ITCZ) through the wind-evaporation-SST feedback (e.g., Lin, 2007; Samanta et al., 2019; J. Lee et al., 2022). In extratropical oceans, SST biases influence storm tracks by altering the meridional temperature gradient (Priestley et al., 2023).

SST biases can also have far-reaching influences (Wang et al., 2014). Recent studies have shown that SST biases in the tropical Pacific and Atlantic Oceans contribute to biases in surface temperature and precipitation over North America (Johnson et al., 2020; Stan et al., 2023). Zhao et al. (2023) showed that SST biases in the tropical Indian Ocean can lead to global atmospheric circulation biases similar to that from steady heating perturbations (e.g., Kosovelj et al., 2019), characterized by the Matsuno-Gill pattern in the tropics and a Rossby wavetrain structure in the extratropics. These circulation biases cause considerable changes in global energy distribution and interannual variance, especially at large scales (zonal wavenumber $k \leq 5$). They found that posi-

tive SST biases in the tropical Indian Ocean increase the energy of tropical waves and reduce the energy of extratropical waves, as well as weaken the interannual variance of both wave types.

On the other hand, the atmospheric response to SST biases probably depends on the atmospheric background state. Previous studies have demonstrated that the atmospheric response to midlatitude SST anomalies is strongly influenced by the background flow and the model's internal variability (Peng et al., 1995; Peng & Robinson, 2001; Peng et al., 2002; Kushnir et al., 2002; Thomson & Vallis, 2018). The mechanism by which the atmospheric background state modulates the atmospheric response to mid-latitude SST anomalies is suggested to be related to the relative latitudinal position of the subtropical jet and the changes in the meridional SST gradient caused by the anomalies (Brayshaw et al., 2008). Likewise, the response to tropical SST anomalies is also modulated by the background state, with studies showing diverse global precipitation responses to SST changes in the tropical Indian Ocean and West Pacific (Barsugli & Sardeshmukh, 2002). Besides, C. Zhou et al. (2017) showed that positive SST anomalies in the tropical ascending and descending regions exert contrasting impacts on low-cloud cover and radiation.

Additionally, the effect of SST biases is expected to depend on the oceanic background state, although research on this subject has so far been limited. G. Zhou et al. (2017) demonstrated that the atmospheric response to an SST anomaly in the extratropical North Pacific is sensitive to decadal variations of background SST. They found that decadal variations of the daily SST variability in the eastern North Pacific and the Oyashio Extension front in the western North Pacific can cause a regime shift in the Rossby wave source associated with the SST anomaly. The present study contributes to this subject by quantifying the effect of regional SST biases on global circulation in relation to background SST. As we will show, the impact of warm SST biases in boreal winter remains local and small unless the background SST is sufficiently high to feed moist processes and precipitation.

SST biases influence the atmosphere through air-sea interactions that are closely related to background SST. An increase in SST locally leads to more upward heat and moisture fluxes, which reduce the moist static stability near the surface and enhance convection (Neelin & Held, 1987). From a thermodynamic perspective, precipitation is more sensitive to SST changes at higher SSTs. This is because SST changes at higher SSTs induce larger perturbations of boundary-layer moist static energy, since low-level atmospheric moisture is expected to increase exponentially with SST (Tory & Dare, 2015). However, many observational and numerical studies have identified a transition to intense convection with SSTs ranging from about 26°C to about 30°C (e.g., Graham & Barnett, 1987; C. Zhang, 1993; Sud et al., 1999; Trenberth & Shea, 2005; Roxy, 2014; He et al., 2018). This suggests that a warm SST bias superimposed on background SST around 26°C or well below this threshold would lead to distinctly different responses. We hypothesize that the transition to intense convection at higher background SSTs, marked by the onset of intense precipitation, is a key factor shaping the atmospheric response to regional SST biases.

The outline of the paper is as follows. Section 2 describes the climate model used and the experimental design, along with a brief introduction to the method for quantifying circulation biases. Section 3 presents our key findings, including analyses of circulation biases, changes in simulated spatio-temporal variability, and discussions on the dependence of the response on background SST. We summarize the study in Section 4.

2 Methodology

2.1 Model and Experiments

A series of numerical experiments are conducted using the Planet Simulator (PLASIM; Fraedrich et al., 2005). PLASIM is a spectral model that employs hydrostatic primitive equations in σ-coordinate to simulate moist atmospheric dynamics. Unresolved processes are parameterized, such as latent and sensible heat fluxes and moist convection. For further details on the model, readers are referred to Fraedrich et al. (2005). PLASIM has been used in numerous studies, such as moist predictability (Rivière et al., 2009), climate change (Lucarini et al., 2010), the effect of aerosol and greenhouse gas forcing on South and East Asian monsoons (Recchia & Lucarini, 2023), extreme events (Herein et al., 2023), atmospheric responses to SST biases (Zhao et al., 2023), among others.

Our simulations employ PLASIM with the prescribed SST and sea ice concentration from the ERA-20C reanalyses (Poli et al., 2016). In our perfect-model framework, the control simulation uses the time-varying monthly mean SST. Sensitivity experiments use the same SST, but with added time-constant perturbations representing SST biases in specific regions around the globe. These perturbations are given as a 2D Gaussian function with a peak of +1.5 K and a full width at half maximum of $40\sqrt{\ln 2}$ degrees in the meridional direction and $30\sqrt{\ln 2}$ degrees in the zonal direction. We generate SST perturbations (i.e., biases) at intervals of 15 degrees from 60°S to 45°N and 20 degrees from 0° to 340°E. After excluding those primarily over land, we obtain 106 distinct SST biases in various ocean regions (see Fig. S1 in Supplementary Information). Note that these biases have the same size in the latitude-longitude coordinate, but their spatial size varies with latitude due to the spherical curvature. For convenience, sensitivity experiments are named after the location of the SST bias; e.g., 'EQ80E' denotes the experiment with the SST bias centered at (0°, 80°E), while '30N220E' refers to the experiment with the SST bias centered at (30°N, 220°E). All experiments run from 1 January 1901 through 31 December 2010, starting with initial conditions from a 40-year spin-up run using the climatological monthly mean ERA-20C SST.

The rest of the model setup is as in Zhao et al. (2023). The model has ten σ levels with a T31 horizontal resolution. Although the applied resolution is not exceptionally high, it is adequate for capturing large-scale circulations, which are of our primary interest. The control simulation has been validated against reanalysis data, as shown in Zhao et al. (2023), confirming the ability of PLASIM to accurately simulate climate states in terms of precipitation and general circulation.

SST biases affect the model atmosphere by modifying surface heat and moisture fluxes. A positive SST bias directly increases the upward sensible heat flux and also enhances the upward moisture flux related to the Clausius–Clapeyron equation. Changes in moisture flux further affect precipitation through the parameterization of cumulus convection in PLASIM (Zhao et al., 2023).

2.2 Evaluation of the effects of SST biases

PLASIM simulations are analyzed using MODES software (Žagar et al., 2015). With MODES, the global fields of wind (u and v) and geopotential height (z) can be simultaneously projected onto the eigensolutions (i.e., normal mode functions) of the linearized primitive equations, yielding circulation in modal space spanned by the zonal wavenumber k, the meridional mode index n and the vertical mode index m. A single normal mode index is denoted $\nu = (k, n, m)$ and the associated complex coefficient of the projection is $\chi_\nu(t)$, which represents the circulation in modal space (see Supplementary Information for details). By simultaneously considering both dynamic and thermodynamic variables, this multivariate projection provides a more complete representation of atmospheric circulation than the univariate projection.

Spatial and temporal variability of the global circulation is evaluated in terms of energy and interannual variance spectra in modal space, respectively. The global mechanical energy (kinetic energy plus available potential energy) per unit area of the mode ν at time t is defined as (Žagar et al., 2020)

$$E_\nu(t) = \frac{1}{2} g D_m \left|\chi_\nu(t)\right|^2, \tag{1}$$

where g is the gravity acceleration, and D_m is the equivalent height of vertical mode m. E_ν has been referred to as the spatial variance (e.g. Žagar et al., 2020). The interannual variance is given by

$$V_\nu = \frac{1}{N} \sum_{t=1}^{N} g D_m \left|\chi_\nu(t) - \overline{\chi_\nu}\right|^2, \tag{2}$$

with N being the number of years and $\overline{\chi_\nu}$ as the mean of $\chi_\nu(t)$ over time.

Changes in spatial and temporal variabilities due to SST bias are evaluated, respectively, as the difference of the time-mean E_ν and V_ν between sensitivity and control simulations, which are denoted by $\Delta\overline{E_\nu} = \overline{E_\nu^S} - \overline{E_\nu^C}$ and $\Delta V_\nu = V_\nu^S - V_\nu^C$. These two metrics provide a quantitative measure of the effect each SST bias has on atmospheric circulation from both spatial and temporal perspectives, enabling us to quantitatively compare the effects of all SST biases. While they allow the analysis of individual modes, in this study, we focus on the globally integrated energy and interannual variance of all wave ($k > 0$) modes in which we are most interested, namely $\overline{E} = \Sigma_{k>0}\Sigma_n\Sigma_m\overline{E_{knm}}$ and $V = \Sigma_{k>0}\Sigma_n\Sigma_m V_{knm}$, respectively. We denote the changes in the globally integrated wave energy and interannual variance as $\Delta\overline{E}$ and ΔV.

3 Results

We first present the circulation sensitivity to regional SST biases in terms of changes in wave ($k > 0$) energy and interannual variance (IAV), before discussing the role of background SST for the observed response. We focus on boreal winter (December-January-February; DJF).

3.1 Circulation and precipitation responses

Figure 1 displays the 250-hPa geopotential height biases and precipitation biases for nine out of the 106 experiments, including three experiments along 30°N (30N140E, 30N220E, 30N320E), the equator (EQ80E, EQ180E, EQ340E), and 30°S (30S80E, 30S220E, 30S340E). The presented experiments exemplify both tropical (Figs. 1d-1f) and extratropical (Figs. 1a-1c and 1g-1i) cases.

SST biases in the tropics lead to considerable global bias teleconnections in geopotential height accompanied by strong precipitation biases (Figs. 1d-1f). In particular, the SST bias at 180°E results in large precipitation biases in the Indo-West Pacific region with a maximum amplitude of over 8 mm day^{-1}, which produces wavetrain patterns in geopotential height in both the North and South Hemispheres (Fig. 1e). In contrast, when the SST bias is in the extratropics, it generally causes small positive precipitation biases locally. Correspondingly, the geopotential height biases are weak (Figs. 1a-1c and 1g-1i). This suggests that the atmospheric response to SST biases depends on the latitude of the bias location.

However, regional extratropical SST biases can still affect circulation in distant areas, even across hemispheres. For instance, the SST bias at (30°N, 140°E) causes significant geopotential height biases along the great circle from East Asia to the North Atlantic. Similarly, the SST bias at (30°S, 80°E) causes significant geopotential height biases over the North Pacific (Fig. 1g), and the SST bias in the South Atlantic causes noticeable geopotential height biases over the North Atlantic (Fig. 1i). These results are

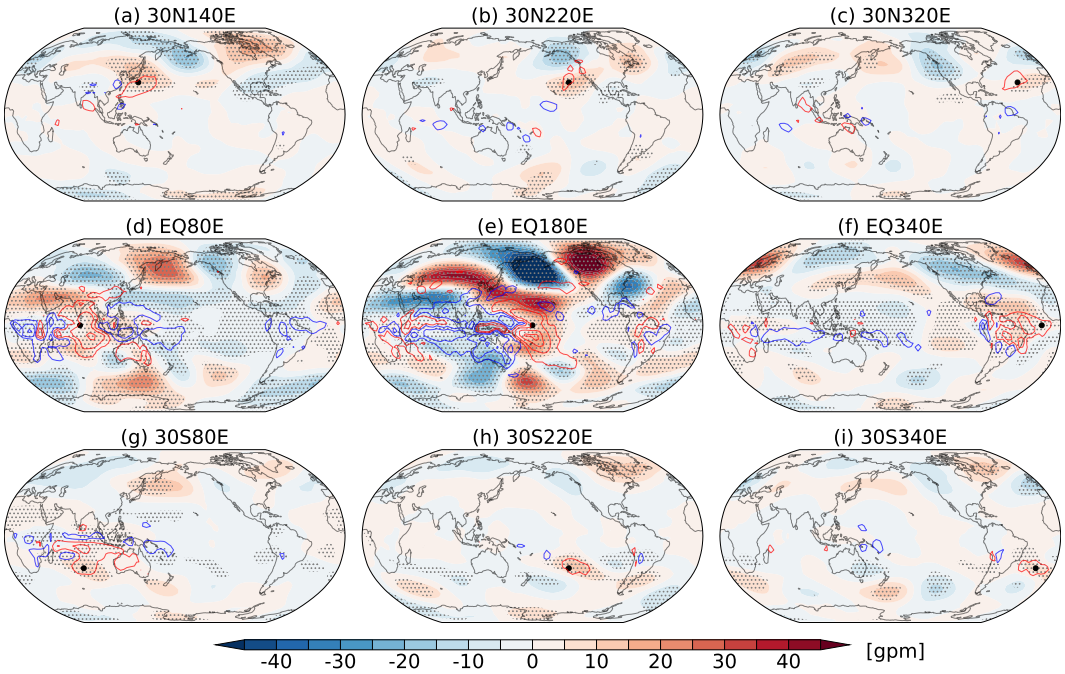

Figure 1. Geopotential height biases (in gpm) at 250 hPa in experiments with SST biases at (a-c) 30°N (30N140E, 30N220E, and 30N320E), (d-f) the equator (EQ80E, EQ180E, and EQ340E), and (g-i) 30°S (30S80E, 30S220E, and 30S340E). The zonal-mean part has been excluded. Dotted areas indicate regions where geopotential height biases are statistically significant at the 0.05 level by Student's t test. Precipitation biases are overlaid with contours at levels: ± 0.5, ± 2, ± 5, and ± 8 mm day^{-1}. Negative contours are shown in blue, and positive contours in red. The large black dot in each panel denotes the SST bias center in the respective experiment.

in line with Thomson and Vallis (2018) who demonstrated that SST anomalies in mid-latitudes usually do not generate a robust response in the free atmosphere, but they can still induce a significant remote response, especially when aligned with internal modes of variability.

The circulation response also varies with the longitude of the SST bias location. We see that SST biases in the Pacific warm pool, such as the experiment EQ180E (Fig. 1e), result in much stronger bias teleconnections than SST biases in the tropical Indian Ocean (Fig. 1d) and Atlantic (Fig. 1f). Differences in the response to tropical SST biases at different longitudes are probably related to the prevalence of ascending and descending motions in the atmosphere above the SST bias. For example, C. Zhou et al. (2017) have shown that SST changes in tropical ascent regions have stronger influences on cloud feedback than those in subsidence regions. Another example is the SST bias located at 30°N to the east of China, which generates a Rossby wavetrain across the North Pacific, North America, and the North Atlantic (Fig. 1a), whereas the SST bias west of North America leads to a meridional dipolar bias in geopotential height (Fig. 1b). SST biases in the extratropical jet stream regions (Figs. 1a) seem more effective in producing Rossby wavetrains than those in areas of weaker background flow (Fig. 1b).

While Figure 1 makes it clear that SST biases at different locations lead to different bias teleconnections, their quantification and comparison call for integrated metrics. Here, we use the globally integrated mechanical energy and IAV. As mentioned earlier, they consider both temperature (i.e. geopotential height) and wind, while also accounting for the spatial and temporal aspects of the circulation response.

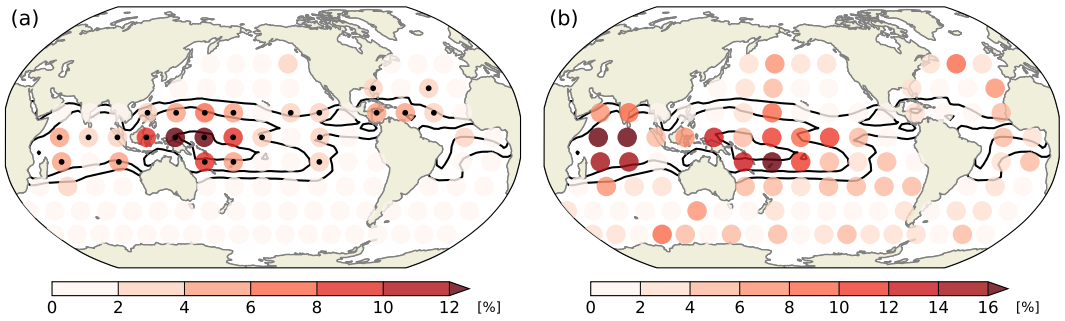

Figure 2. Relative changes (in %) of the global wave (k>0) energy and IAV in DJF with respect to the control simulation: (a) $|\Delta\overline{E}/\overline{E^C}|$ and (b) $|\Delta V/V^C|$. Each dot denotes one experiment with the respective SST bias centered at the dot. Small black dots in (a) denote significance at the 0.05 level by Student's t test. Note that the significance of the IAV changes can be examined for each mode, however, it is not possible to do so for the globally integrated quantity, as shown in (b). Black contours overlaid show the climotological SST at 25, 27, and 29°C for the respective season. See the text for details.

Figure 2 shows the relative changes in global wave energy and IAV due to each SST bias. Note that each dot gives the global, rather than the local, changes resulting from the SST bias centered at the respective location. The relative changes are calculated by dividing the absolute changes by the respective reference states of the control run, denoted $|\Delta\overline{E}/\overline{E^C}|$ and $|\Delta V/V^C|$, respectively. In fact, the changes are either positive or negative (see Fig. S2 in Supplementary Information). The sign of the changes indicates modulation of the atmospheric background state, which is beyond the scope of this paper. Therefore, only their magnitudes are shown. The significance of global energy changes is easily checked, whereas that for the IAV changes is not feasible as it only applies to individual modes.

First, we look at the changes in global wave energy (Fig. 2a). In general, SST biases in the tropics result in larger changes in wave energy than SST biases in the extratropics. Moreover, there appears to be a transition between the tropical and extratropical experiments, following the 25°C isoline of the background SST. Very strong responses to SST biases are observed in areas where the background SST exceeds about 25°C. The strongest response is observed in the Pacific warm pool, with experiments EQ140E and EQ160E showing the largest values, exceeding 12%. On the contrary, responses are generally weak, less than 2% of the reference state, when SST biases occur in regions where the background SST is below 25°C. In other words, the impact of tropical SST biases on global wave energy can be more than six times greater than that of extratropical SST biases.

However, not all strong responses are seen in warm SST regions. For instance, SST biases in experiments 30N280E and 30N320E, which are located in the North Atlantic, still lead to significant changes in wave energy. Furthermore, some tropical SST biases in regions with warm background SST have very weak global impacts, such as those in the eastern Pacific and Atlantic. The decoupling between the response amplitude and background SST in these cases should be related to the local atmospheric background state.

Changes in IAV further highlight the relationship with background SST (Fig. 2b). The strongest changes are caused by SST biases in the tropical Indo-West Pacific region, whereas SST biases in relatively cold SST regions have weak impacts on IAV. There are some notable differences between the IAV response and the energy response. One is observed in the tropical Indian Ocean, where SST biases lead to very large IAV changes, which can exceed 16% of the reference state. However, the energy changes are relatively small, though significant, at less than 6% of the reference state. In addition, some extratropical SST biases can exert relatively larger impacts on IAV (which can exceed 6% of the reference state) than on energy (which is generally less than 2% of the reference state), such as those in the North Pacific, North America and along the Antarctic coast. The difference between the energy response and the IAV response is expected, since energy and IAV represent two distinct aspects of variability. However, a complete understanding of these differences has not yet been achieved.

So far, we have demonstrated a strong correlation between the atmospheric response to regional SST biases on background SST. In the following, we will explain how this dependence occurs.

3.2 Mechanism of the dependence on background SST

SST biases affect the model atmosphere through air-sea interactions. A positive SST bias generally leads to locally more upward sensible heat flux and moisture flux, which reduce the near-surface moist static stability (Neelin & Held, 1987), leading to local positive precipitation biases. As seen in Fig. 1, positive SST biases typically increase local precipitation. The accompanying latent heat release drives the circulation response. In general, the greater the increase in local precipitation over the positive SST bias, the stronger the local and remote response. Therefore, the problem of coupling atmospheric circulation bias teleconnections with SST biases is equivalent to understanding the dependence of local precipitation changes on background SST.

Figure 3a shows the local precipitation change for each SST bias, denoted ΔPr. It is calculated as the mean precipitation bias in areas where the respective SST bias is greater than 0.5 K. The ΔPr pattern is very similar to the pattern of energy changes (Fig. 2a). This indicates that tropical SST biases result in much greater ΔPr than extratropical SST biases, which generally result in ΔPr smaller than 0.5 mm day^{-1}. The transition from large ΔPr in the tropics to small ΔPr in the extratropics closely follows 25°C isoline of the background SST. In Fig. 3b, ΔPr is presented as a function of the

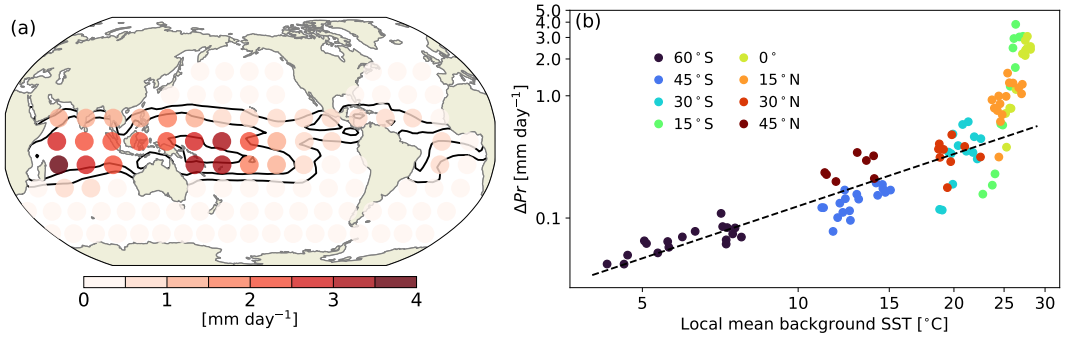

Figure 3. (a) Same as Fig. 2a, but for local precipitation changes (ΔPr, in mm day^{-1}). For each experiment, ΔPr is calculated as the average within the area of the respective SST bias. Panel (b) shows ΔPr as a function of the local background SST (in °C), which is calculated as the average within the area of the respective SST bias. The dot color indicates the central latitude of the SST bias. The straight line is a best fit to the data below 25°C SST. See the text for details.

local background SST in a log-log plot. It shows that when the local background SST is below 25°C, ΔPr approximately collapses on a straight line, implying a power-law relationship. However, when the local background SST is above 25°C, ΔPr departs from the line (i.e., from the power law), implying the transition from one behavior (i.e., small precipitation increase) to other types of relationship (abnormally large increase) in the system. This actually indicates the transition from shallow to deep convection as a positive SST bias is superimposed, since changes in precipitation indicate changes in convection. This kind of critical phenomenon has been studied by Peters and Neelin (2006).

Based on Fig. 3, we can now discuss the mechanism behind changes in global wave energy and IAV in relation to background SST. Their dependence is evidently mediated by the precipitation response to the SST bias. Local precipitation biases explain the response amplitude of $|\Delta\overline{E}|$ and $|\Delta V|$. A larger ΔPr leads to increased latent heat release, intensifying Rossby wave sources and, consequently, amplifying $|\Delta\overline{E}|$ and $|\Delta V|$. The sharp change of ΔPr near a background SST of about 25°C is also reflected in $|\Delta\overline{E}|$ and $|\Delta V|$ (see Fig. 2 and Fig. S3 in Supplementary Information). The pointwise correlation between $|\Delta\overline{E}|$ (Fig. 2a) and ΔPr (Fig. 3a) is 0.75 and 0.67 between $|\Delta V|$ (Fig. 2b) and ΔPr (Fig. 3a). This means that ΔPr alone explains 56% of the spatial pattern of $|\Delta\overline{E}|$ and 45% of the spatial pattern of $|\Delta V|$. Obviously, $|\Delta\overline{E}|$ and $|\Delta V|$ cannot be exclusively attributed to ΔPr, since nonlinear dynamics is involved. As shown in Zhao et al. (2023), the wave energy and IAV in the extratropics dominate those in the tropics. In the extratropics, the interaction between waves and the zonal mean flow plays a key role in modulating both wave energy and IAV (e.g., Zhao & Liang, 2018), which is independent of ΔPr. In addition, the more intricate pattern (with a smaller correlation with ΔPr) of the IAV response is probably related to the atmospheric background state, especially the internal variability of the circulation, as suggested by Thomson and Vallis (2018). When the forced mode by SST biases aligns with the internal modes of variability, the variability response is strong. This may account for the significant changes in IAV caused by extratropical SST biases (see Fig. 2b).

4 Conclusions

Based on extensive numerical experiments with a general circulation model, this study examined the global atmospheric circulation response to the positive SST bias as

a function of its location. Despite its low resolution, the model simulates large-scale dynamics well. The model employs parameterizations of physical processes, such as surface fluxes and cumulus convection, as in many complex climate models, and the moist processes are well represented. Results were analyzed using the multivariate projection, which enables us to quantify the response from both the dynamic and thermodynamic perspectives, providing a unified insight into changes in the general circulation.

Key findings include:

1. SST biases, even if they are of identical size and amplitude, can exert varying effects on the simulated atmospheric circulation depending on their geographic location. The impact of tropical SST biases is found to be far more pronounced — potentially more than six times greater — than that of extratropical SST biases, particularly in terms of changes in the global wave energy and interannual variance.
2. The geographic dependence is largely dictated by background SST, with notable effects occurring when the bias (with an amplitude of +1.5 K) is located in regions where the background SST exceeds approximately 25°C. The Indo-West Pacific warm pool is particularly sensitive.
3. Dependency of the atmospheric circulation response on the background SST is determined by the local precipitation response, which is associated with the critical SST threshold for intense convection. When a +1.5 K SST bias superimposed on the background SST exceeds the threshold, excessive local precipitation and latent heat release cause a strong response in atmospheric circulation.

These findings highlight the intricate interplay between regional SST biases, local precipitation responses, and atmospheric circulation responses, emphasizing the sensitivity of certain regions such as the Indo-West Pacific warm pool to positive SST biases. Considering that most CMIP models have suffered from severe SST biases over time (Davey et al., 2002; Huang et al., 2007; Xu et al., 2014; Toniazzo & Woolnough, 2014; Richter, 2015; Q. Zhang et al., 2023; Stan et al., 2023), an implication is that relatively more attention should be paid to tropical oceans, especially the Indo-West Pacific, where SST biases can produce large bias teleconnections and greatly deteriorate the usability of global climate simulations.

Furthermore, whether we are talking about SST biases or SST anomalies, the underlying physical processes are essentially the same. Therefore, the results of this study have broader implications for understanding how the atmosphere responds to regional SST changes.

Although most extratropical SST biases were found not to lead to a robust global response, they still have significant regional impacts (see Fig. 1). Also, remember that an increase in the magnitude of the SST bias or the model resolution may enhance the overall responses (e.g., Boville, 1991; Kushnir et al., 2002; R. W. Lee et al., 2018; G. Zhou, 2019).

We discussed only absolute changes in the global wave energy and interannual variance. In fact, the sign of the response varies across ocean basins, implying modulation by the atmospheric background state. Furthermore, we have not discussed the effects on different dynamical regimes and scales, including the zonal mean state, as conducted by (Zhao et al., 2023). Scale and regime dependency, and variations of the sign of response across ocean basins are the subject of the follow-on paper.

Open Research Section

Monthly SST data used in this study are publicly available (Poli et al., 2016). All data presented in this paper can be downloaded from `https://doi.org/10.5281/zenodo.10477872`. Information on PLASIM model is available at `https://www.mi.uni-hamburg.de/en/arbeitsgruppen/theoretische-meteorologie/modelle/plasim.html`. The MODES package can be requested via `https://modes.cen.uni-hamburg.de`.

Acknowledgments

The authors thank Dr. Richard Blender for helpful discussions. This work is a contribution to Project S1 of the Collaborative Research Centre TRR 181 "Energy Transfer in Atmosphere and Ocean" funded by the Deutsche Forschungsgemeinschaft (DFG, German Research Foundation) under project number 274762653.

References

Barsugli, J. J., & Sardeshmukh, P. D. (2002). Global atmospheric sensitivity to tropical sst anomalies throughout the indo-pacific basin. *Journal of Climate*, *15*(23), 3427–3442. doi: 10.1175/1520-0442(2002)015⟨3427:GASTTS⟩2.0.CO;2

Boville, B. A. (1991). Sensitivity of simulated climate to model resolution. *Journal of Climate*, *4*(5), 469–485. doi: 10.1175/1520-0442(1991)004⟨0469:SOSCTM⟩2.0.CO;2

Brayshaw, D. J., Hoskins, B., & Blackburn, M. (2008). The storm-track response to idealized sst perturbations in an aquaplanet gcm. *Journal of the Atmospheric Sciences*, *65*(9), 2842–2860. doi: 10.1175/2008JAS2657.1

Burls, N. J., Muir, L., Vincent, E. M., & Fedorov, A. (2017). Extra-tropical origin of equatorial pacific cold bias in climate models with links to cloud albedo. *Climate Dynamics*, *49*(5), 2093–2113. doi: 10.1007/s00382-016-3435-6

Davey, M., Huddleston, M., Sperber, K., Braconnot, P., Bryan, F., Chen, D., ... others (2002). Stoic: a study of coupled model climatology and variability in tropical ocean regions. *Climate Dynamics*, *18*, 403–420. doi: 10.1007/s00382-001-0188-6

Fraedrich, K., Jansen, H., Kirk, E., Luksch, U., & Lunkeit, F. (2005). The planet simulator: Towards a user friendly model. *Meteorologische Zeitschrift*, 299–304. doi: 10.1127/0941-2948/2005/0043

Graham, N. E., & Barnett, T. P. (1987). Sea surface temperature, surface wind divergence, and convection over tropical oceans. *Science*, *238*(4827), 657–659. doi: 10.1126/science.238.4827.657

He, J., Johnson, N. C., Vecchi, G. A., Kirtman, B., Wittenberg, A. T., & Sturm, S. (2018). Precipitation sensitivity to local variations in tropical sea surface temperature. *Journal of Climate*, *31*(22), 9225–9238. doi: 10.1175/JCLI-D-18-0262.1

Herein, M., Jánosi, D., & Tél, T. (2023). An ensemble based approach for the effect of climate change on the dynamics of extremes. *Frontiers in Earth Science*, *11*, 1267473. doi: 10.3389/feart.2023.1267473

Huang, B., Hu, Z.-Z., & Jha, B. (2007). Evolution of model systematic errors in the tropical atlantic basin from coupled climate hindcasts. *Climate dynamics*, *28*, 661–682. doi: 10.1007/s00382-006-0223-8

Johnson, N. C., Krishnamurthy, L., Wittenberg, A. T., Xiang, B., Vecchi, G. A., Kapnick, S. B., & Pascale, S. (2020). The impact of sea surface temperature biases on north american precipitation in a high-resolution climate model. *Journal of Climate*, *33*(6), 2427–2447. doi: 10.1175/JCLI-D-19-0417.1

Joseph, S., Sahai, A. K., Goswami, B. N., Terray, P., Masson, S., & Luo, J.-J. (2012). Possible role of warm SST bias in the simulation of boreal summer

monsoon in SINTEX-f2 coupled model. *Climate Dynamics*, *38*(7), 1561–1576. doi: 10.1007/s00382-011-1264-1

Kosovelj, K., Kucharski, F., Molteni, F., & Žagar, N. (2019). Modal decomposition of the global response to tropical heating perturbations resembling MJO. *Journal of the Atmospheric Sciences*, *76*(5), 1457–1469. doi: 10.1175/JAS-D-18-0203.1

Kushnir, Y., Robinson, W., Bladé, I., Hall, N., Peng, S., & Sutton, R. (2002). Atmospheric gcm response to extratropical sst anomalies: Synthesis and evaluation. *Journal of Climate*, *15*(16), 2233–2256. doi: 10.1175/1520-0442(2002)015⟨2233:AGRTES⟩2.0.CO;2

Lee, J., Kang, S. M., Kim, H., & Xiang, B. (2022). Disentangling the effect of regional SST bias on the double-ITCZ problem. *Climate Dynamics*, *58*(11), 3441–3453. doi: 10.1007/s00382-021-06107-x

Lee, R. W., Woollings, T. J., Hoskins, B. J., Williams, K. D., O'Reilly, C. H., & Masato, G. (2018). Impact of gulf stream sst biases on the global atmospheric circulation. *Climate Dynamics*, *51*, 3369–3387. doi: 10.1007/s00382-018-4083-9

Lin, J.-L. (2007). The double-ITCZ problem in IPCC AR4 coupled GCMs: Ocean-tmosphere feedback analysis. *Journal of Climate*, *20*(18), 4497–4525. doi: 10.1175/JCLI4272.1

Lucarini, V., Fraedrich, K., & Lunkeit, F. (2010). Thermodynamics of climate change: generalized sensitivities. *Atmospheric Chemistry and Physics*, *10*(20), 9729–9737. doi: 10.5194/acp-10-9729-2010

Neelin, J. D., & Held, I. M. (1987). Modeling tropical convergence based on the moist static energy budget. *Monthly Weather Review*, *115*(1), 3–12. doi: 10.1175/1520-0493(1987)115⟨0003:MTCBOT⟩2.0.CO;2

Peng, S., Mysak, L., Derome, J., Ritchie, H., & Dugas, B. (1995). The differences between early and midwinter atmospheric responses to sea surface temperature anomalies in the northwest atlantic. *Journal of Climate*, *8*(2), 137–157. doi: 10.1175/1520-0442(1995)008⟨0137:TDBEAM⟩2.0.CO;2

Peng, S., & Robinson, W. A. (2001). Relationships between atmospheric internal variability and the responses to an extratropical sst anomaly. *Journal of climate*, *14*(13), 2943–2959. doi: 10.1175/1520-0442(2001)014⟨2943:RBAIVA⟩2.0.CO;2

Peng, S., Robinson, W. A., & Li, S. (2002). North atlantic sst forcing of the nao and relationships with intrinsic hemispheric variability. *Geophysical Research Letters*, *29*(8), 117-1. doi: 10.1029/2001GL014043

Peters, O., & Neelin, J. D. (2006). Critical phenomena in atmospheric precipitation. *Nature physics*, *2*(6), 393–396. doi: 10.1038/nphys314

Poli, P., Hersbach, H., Dee, D. P., Berrisford, P., Simmons, A. J., Vitart, F., ... Fisher, M. (2016). ERA-20c: An atmospheric reanalysis of the twentieth century. *Journal of Climate*, *29*(11), 4083 – 4097. doi: 10.1175/JCLI-D-15-0556.1

Priestley, M. D. K., Ackerley, D., Catto, J. L., & Hodges, K. I. (2023). Drivers of biases in the CMIP6 extratropical storm tracks. part i: Northern hemisphere. *Journal of Climate*, *36*(5), 1451–1467. doi: 10.1175/JCLI-D-20-0976.1

Prodhomme, C., Terray, P., Masson, S., Izumo, T., Tozuka, T., & Yamagata, T. (2014). Impacts of indian ocean SST biases on the indian monsoon: as simulated in a global coupled model. *Climate Dynamics*, *42*(1), 271–290. doi: 10.1007/s00382-013-1671-6

Recchia, L. G., & Lucarini, V. (2023). Modelling the effect of aerosol and greenhouse gas forcing on the south asian and east asian monsoons with an intermediate-complexity climate model. *Earth System Dynamics*, *14*(3), 697–722. doi: 10.5194/esd-14-697-2023

Richter, I. (2015). Climate model biases in the eastern tropical oceans: Causes,

impacts and ways forward. *Wiley Interdisciplinary Reviews: Climate Change*, *6*(3), 345–358. doi: 10.1002/wcc.338

Rivière, O., Lapeyre, G., & Talagrand, O. (2009). A novel technique for nonlinear sensitivity analysis: Application to moist predictability. *Quarterly Journal of the Royal Meteorological Society*, *135*(643), 1520–1537. doi: 10.1002/qj.460

Roxy, M. (2014). Sensitivity of precipitation to sea surface temperature over the tropical summer monsoon region—and its quantification. *Climate Dynamics*, *43*(5), 1159–1169. doi: 10.1007/s00382-013-1881-y

Samanta, D., Karnauskas, K. B., & Goodkin, N. F. (2019). Tropical pacific SST and ITCZ biases in climate models: Double trouble for future rainfall projections? *Geophysical Research Letters*, *46*(4), 2242–2252. doi: 10.1029/2018GL081363

Stan, C., Krishnamurthy, V., Bai, H., Li, B., Mehra, A., Meixner, J., ... Yang, F. (2023). The impact of tropical pacific SST biases on the s2s forecast skill over north america in the UFS global coupled model. *Journal of Climate*, *36*(8), 2439–2456. doi: 10.1175/JCLI-D-22-0196.1

Sud, Y. C., Walker, G. K., & Lau, K. M. (1999). Mechanisms regulating sea-surface temperatures and deep convection in the tropics. *Geophysical Research Letters*, *26*(8), 1019–1022. doi: 10.1029/1999GL900197

Thomson, S. I., & Vallis, G. K. (2018). Atmospheric response to SST anomalies. part i: Background-state dependence, teleconnections, and local effects in winter. *Journal of the Atmospheric Sciences*, *75*(12), 4107–4124. doi: 10.1175/JAS-D-17-0297.1

Toniazzo, T., & Woolnough, S. (2014). Development of warm sst errors in the southern tropical atlantic in cmip5 decadal hindcasts. *Climate dynamics*, *43*, 2889–2913. doi: 10.1007/s00382-013-1691-2

Tory, K. J., & Dare, R. A. (2015). Sea surface temperature thresholds for tropical cyclone formation. *Journal of Climate*, *28*(20), 8171–8183. doi: 10.1175/JCLI-D-14-00637.1

Trenberth, K. E., & Shea, D. J. (2005). Relationships between precipitation and surface temperature. *Geophysical Research Letters*, *32*(14). doi: 10.1029/2005GL022760

Wang, C., Zhang, L., Lee, S.-K., Wu, L., & Mechoso, C. R. (2014). A global perspective on CMIP5 climate model biases. *Nature Climate Change*, *4*(3), 201–205. doi: 10.1038/nclimate2118

Wills, R. C. J., Dong, Y., Proistosecu, C., Armour, K. C., & Battisti, D. S. (2022). Systematic climate model biases in the large-scale patterns of recent sea-surface temperature and sea-level pressure change. *Geophysical Research Letters*, *49*(17), e2022GL100011. doi: 10.1029/2022GL100011

Xu, Z., Chang, P., Richter, I., Kim, W., & Tang, G. (2014). Diagnosing southeast tropical atlantic sst and ocean circulation biases in the cmip5 ensemble. *Climate dynamics*, *43*, 3123–3145. doi: 10.1007/s00382-014-2247-9

Žagar, N., Kasahara, A., Terasaki, K., Tribbia, J., & Tanaka, H. (2015). Normal-mode function representation of global 3-D data sets: open-access software for the atmospheric research community. *Geoscientific Model Development*, *8*(4), 1169-1195. doi: 10.5194/gmd-8-1169-2015

Žagar, N., Kosovelj, K., Manzini, E., Horvat, M., & Castanheira, J. (2020). An assessment of scale-dependent variability and bias in global prediction models. *Climate Dynamics*, *54*(1), 287–306. doi: 10.1007/s00382-019-05001-x

Zhang, C. (1993). Large-scale variability of atmospheric deep convection in relation to sea surface temperature in the tropics. *Journal of Climate*, *6*(10), 1898–1913. doi: 10.1175/1520-0442(1993)006⟨1898:LSVOAD⟩2.0.CO;2

Zhang, Q., Liu, B., Li, S., & Zhou, T. (2023). Understanding models' global sea surface temperature bias in mean state: From cmip5 to cmip6. *Geophysical Research Letters*, *50*(4), e2022GL100888. doi: https://doi.org/10.1029/2022GL100888

Zhao, Y.-B., & Liang, X. S. (2018). On the inverse relationship between the boreal wintertime Pacific jet strength and storm-track intensity. *Journal of Climate*, *31*(23), 9545 - 9564. doi: 10.1175/JCLI-D-18-0043.1

Zhao, Y.-B., Žagar, N., Lunkeit, F., & Blender, R. (2023). Atmospheric bias teleconnections associated with systematic sst errors in the tropical indian ocean. *Weather and Climate Dynamics*. doi: 10.5194/egusphere-2023-917

Zhou, C., Zelinka, M. D., & Klein, S. A. (2017). Analyzing the dependence of global cloud feedback on the spatial pattern of sea surface temperature change with a green's function approach. *Journal of Advances in Modeling Earth Systems*, *9*(5), 2174–2189. doi: 10.1002/2017MS001096

Zhou, G. (2019). Atmospheric response to sea surface temperature anomalies in the mid-latitude oceans: A brief review. *Atmosphere-Ocean*, *57*(5), 319–328. doi: 10.1080/07055900.2019.1702499

Zhou, G., Latif, M., Greatbatch, R. J., & Park, W. (2017). State dependence of atmospheric response to extratropical north pacific sst anomalies. *Journal of Climate*, *30*(2), 509–525. doi: 10.1175/JCLI-D-15-0672.1

Zhu, Y., Zhang, R.-H., & Sun, J. (2020). North pacific upper-ocean cold temperature biases in CMIP6 simulations and the role of regional vertical mixing. *Journal of Climate*, *33*(17), 7523–7538. doi: 10.1175/JCLI-D-19-0654.1